Probing muonic forces with neutron star binaries

Jeff A. Dror,[1,2,*] Ranjan Laha[3,†] and Toby Opferkuch[3,‡]

[1]*Theory Group, Lawrence Berkeley National Laboratory, Berkeley, California 94720, USA*
[2]*Berkeley Center for Theoretical Physics, University of California, Berkeley, California 94720, USA*
[3]*Theoretical Physics Department, CERN, 1211 Geneva, Switzerland*

We show that gravitational wave emission from neutron star binaries can be used to discover any generic long-ranged muonic force due to the large inevitable abundance of muons inside neutron stars. As a minimal consistent example, we focus on a gauged $U(1)_{L_\mu - L_\tau}$ symmetry. In pulsar binaries, such $U(1)_{L_\mu - L_\tau}$ vectors induce an anomalously fast decay of the orbital period through the emission of dipole radiation. We study a range of different pulsar binaries, finding the most powerful constraints for vector masses below $\mathcal{O}(10^{-18} \text{ eV})$. For merging binaries, the presence of muons in neutron stars can result in dipole radiation as well as a modification of the chirp mass during the inspiral phase. We make projections for a prospective search using both the GW170817 and S190814bv events and find that current data can discover light vectors with masses below $\mathcal{O}(10^{-10} \text{ eV})$. In both cases, the limits attainable with neutron stars reach gauge coupling $g' \lesssim 10^{-20}$, which are many orders of magnitude stronger than previous constraints. We also show projections for next generation experiments, such as Einstein Telescope and Cosmic Explorer.

I. INTRODUCTION

New long range interactions give rise to distinctive signatures in a wide range of observables. Such interactions are, however, strongly constrained by fifth-force tests [1–4], unless they are either screened or the couplings to the first generation fermions are suppressed. We show that the dynamics of neutron star (NS) binaries provide ideal laboratories to probe long range muonic forces due to the significant abundance of muons inside them (by mass $\gtrsim 0.1\% \, M_\odot$). The observations of the NS merger event, GW170817 [5], an NS-black hole (BH) candidate merger event, S190814bv [6,7], and various pulsar binaries [8–17] give us the opportunity to probe these new exotic forces. These methods of probing muonic forces via NS binaries are completely general, applicable to both vector and scalar mediators. However, as a concrete realization, we focus on a long-range gauged $U(1)$ symmetry.

Additional $U(1)$ gauge symmetries with masses below the weak scale are simple extensions of Standard Model that can act as a mediator to the dark sector (see, e.g.,

[18–21]), are common predictions of string theory [22], and can explain experimental anomalies [23–28]. The observed matter content limits the linearly independent conserved currents to $B - L$, hypercharge (equivalent to kinetic mixing), and (up to neutrino masses) $L_e - L_\mu$, $L_\mu - L_\tau$, and $L_e - L_\tau$.[1] The small number of possibilities highlights the need to find all experimental ways to probe these light vectors. While most of the focus when studying the phenomenology of new $U(1)$ gauge symmetries has been above the eV scale, it is interesting to study the constraints for lighter masses, where forces are long-ranged. For $B - L$, $L_e - L_\mu$, and $L_e - L_\tau$, the constraints below this scale become extremely powerful from fifth force tests [1–4] which constrains such forces to be weaker than gravity once the vector mass drops below $\mathcal{O}(10^{-4} \text{ eV})$ and constraining the gauge coupling $g' \lesssim 10^{-20}$ at the lowest masses. Kinetically mixed dark photons do not experience such constraints due to screening of the charge between protons and electrons leading to rich phenomenology at low masses (see, e.g., [32] and references therein). Interestingly, $L_\mu - L_\tau$ forces also are not bound by these constraints since the muon fraction in ordinary matter is negligible.

For vector masses above an MeV, the strongest constraints on $L_\mu - L_\tau$ range from beam dump experiments,

---

[*]jdror@lbl.gov
[†]ranjan.laha@cern.ch
[‡]toby.opferkuch@cern.ch

---

[1]Relaxing the requirement of anomaly cancellation with just the Standard Model fields greatly enlarges the possibilities but is highly constrained from searches for flavor changing neutral currents [29–31].

muonic $g-2$ measurements, neutrino trident processes, and collider experiments (see, e.g., [28,33–48]). For lower vector masses, the best published constraints on $L_\mu - L_\tau$ arise from $\Delta N_{\rm eff}$ through observations of big bang nucleosynthesis [49,50], from SN1987A [51],[2] and neutrino self-interactions [53–55] constraining $g' \lesssim 10^{-5}$.[3] Such searches are inherently much weaker than searches for long range forces as they do not scale with the size of the apparatus, which will allow us to present constraints much stronger than in previous work. Alternatively, if there exists a mass mixing between the Standard Model Z boson and the new vector, $\mathcal{L} \supset \epsilon_Z m_Z^2 X_\mu Z^\mu$, it can induce a long-range force that would have been observed in neutrino oscillations unless $\epsilon_Z g' \lesssim 10^{-52}$ [42]. However, since a mass mixing can only arise after gauge symmetry breaking, it is naturally small and is highly constrained experimentally [56].

The existence of NSs is contingent entirely on the stability of the neutron through sufficient Pauli blocking of the process $n \to p + e^- + \bar{\nu}_e$ [57–61]. As the neutron density increases similar processes involving muons, rather than electrons, become energetically favorable. This leads to the production of a significant number of muons and forbids their subsequent decay [62]. NSs with masses of order a solar mass subsequently have 0.15%–0.75% of their mass stored in muons, providing a unique laboratory to test couplings of muons to light new degrees of freedom. This has been leveraged to place constraints on muon-philic dark matter due to its accretion in NSs [45,63,64].

A key feature of this muon population is their asymmetric nature, i.e., the production of only muons and not antimuons. Consequently, the presence of new long-range forces coupled to muons leads to NSs acquiring large effective charges. The coupling we are interested in constraining is that of $L_\mu - L_\tau$,

$$\mathcal{L} \supset g' V_\alpha (\bar{\mu}\gamma^\alpha \mu - \bar{\tau}\gamma^\alpha \tau + \bar{\nu}_\mu \gamma^\alpha \nu_\mu - \bar{\nu}_\tau \gamma^\alpha \nu_\tau), \quad (1)$$

where V_α and g' denote the new vector and its coupling strength. We will rely on the couplings to muons as NSs contain negligible numbers of taus or neutrinos. Extending the constraints we derive here to a scalar force is straightforward, where $\mathcal{O}(1)$ changes are expected in the limits on the coupling relative to the vector case.

The observation of gravitational waves (GWs) from NS-NS/NS-BH mergers as well as timing measurements of binary pulsars provides exquisite sensitivity to not only these scenarios, but also many types of dark matter candidates (see [65] and references therein). In both cases, GWs are the dominant energy loss mechanism required to describe the dynamics of the system. For the case of

---

[2]The robustness of the supernova bounds has recently been called into question in [52].

[3]If we insist on a reheating temperature above the muon mass, then there is a stronger bound of $g' \lesssim 10^{-9}$ [47].
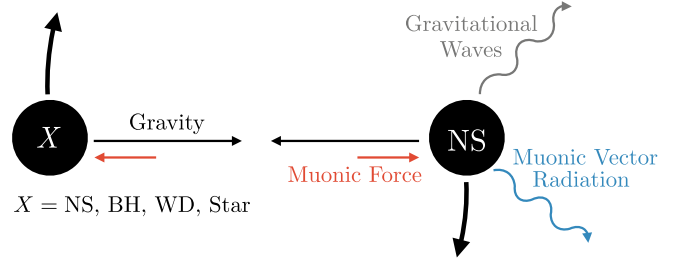
FIG. 1. Sketch of an NS binary system showing the modifications induced by a generic muonic repulsive force and the radiation of the force mediator. Note that the force between the bodies is only present for the case of an NS-NS binary, i.e., $X = NS$.

mergers, sensitivity arises from the long observation duration of the post-Newtonian stage of the GW signal [5]. While for the case of binary pulsars, precise measurements of the change in pulsar period yield accurate determinations of both the relativistic corrections to the binary orbits and the orbital decay (see, e.g., [66]). Therefore, both of these systems are sensitive to additional energy loss mechanisms through the emission of the light vector, while NS mergers are also sensitive to an additional force sourced between the muon content of the two NSs; see Fig. 1. These effects have been studied in the context of new long-range forces in a hidden sector [67–75]. In what follows, we consider the impact a gauged $U(1)_{L_\mu - L_\tau}$ symmetry can have on NS binaries.

II. MUONS IN NEUTRON STARS

The presence of muons in NSs arises due to chemical equilibrium and charge neutrality maintained via the processes $n \to p + e^-/\mu^- + \bar{\nu}_{e/\mu}$ and $e^- \to \mu^- + \bar{\nu}_\mu + \nu_e$, referred to as beta equilibrium. The existence of muons in NSs follows from estimating the Fermi energy of a neutron gas, $E_F = (3\pi^2 n_n)^{2/3}/2m_n$ (where m_n and n_n are the nucleon mass and number density of the neutrons, respectively). NS masses around a solar mass and radius of 10 km give typical Fermi energies of order 100 MeV, suggesting a significant muon abundance.

In the absence of the gauged $U(1)_{L_\mu - L_\tau}$ symmetry, the muon abundance is determined purely by local chemical equilibrium between electrons and muons, namely, $\mu_e(r) = \mu_\mu(r)$, where $\mu_\ell(r) \equiv \sqrt{m_\ell^2 + (3\pi^2 n_\ell(r))^{2/3}}$ (see, for example, Ref. [76]). Inclusion of the gauged $U(1)_{L_\mu - L_\tau}$ symmetry perturbs this picture inducing an unscreened electric field experienced by the muons. This leads to the following integral equation for the chemical potential:

$$\mu_e(r) = \mu_\mu(r) + g'^2 \int_\infty^r dr' \frac{1}{r'^2} \int_0^{r'} dr'' r''^2 n_\mu(r''). \quad (2)$$

This new potential term encompasses the additional energy cost of producing a muon, suppressing their production in

the core of the NS. Given $n_e(r)$, one can then solve this equation for $n_\mu(r)$ to extract the muon number of an NS. In the limit where the potential term is negligible, the equation can be inverted to find $n_\mu(r)$ permitting a simple solution. This will be a good approximation when $g'^2 N_\mu/4\pi r_{NS} \ll \mu_e$, where r_{NS} and N_μ are the radius and the total muon number of the NS, respectively. In the absence of an $L_\mu - L_\tau$ force, N_μ is of order 1% for typical NS parameters meaning for $g' \gtrsim 10^{-18}$ one can no longer neglect the $L_\mu - L_\tau$ force contribution to Eq. (2). However, the muon abundance does not entirely disappear for larger gauge coupling. Muons will continue to be produced in the NS until the point at which the energy stored in the $L_\mu - L_\tau$ field becomes of order the total energy stored in the electron gas, i.e.,

$$\int_V dV E_\mu^2 \lesssim N_e \mu_e \Rightarrow N_\mu \propto 1/g', \qquad (3)$$

where we have approximated the $L_\mu - L_\tau$ electric field as $E_\mu \sim g' N_\mu/r^2$, and N_e is the total number of electrons in the NS. We therefore conclude that N_μ is constant for $g' \lesssim 10^{-18}$ after which it then scales $\propto 1/g'$. However, the observables of interest depend on the total muonic charge of the astrophysical objects, $g' N_\mu$, which for $g' > 10^{-18}$ will subsequently asymptote to a constant value. For the remainder of this paper, we will focus on the case where $g' \lesssim 10^{-18}$, with a detailed derivation of the total muon number given in Appendix A, postponing the larger gauge coupling scenario to future work.

III. NEUTRON STAR BINARY MERGERS

A new muonic force can have a dramatic effect on NS-NS and NS-BH binaries. In the absence of exotic forces, the dynamics of these inspirals are determined by gravitational attraction and emission of gravitational waves. Any new exotic force changes the dynamics in two different ways: (i) the Yukawa force between the muon cores can accelerate or decelerate the merger, and (ii) the emission of the mediator particle increases the energy loss of the system and accelerates the merger. For concreteness, we consider a repulsive force mediated by a vector boson and follow the techniques advocated in [70]. In this section, we outline the technique via which we derive our new constraints. We postpone the detailed formulas to Appendix B.

If the muonic charges carried by the two astrophysical objects are denoted by q_1 and q_2, then the Yukawa force between them can be written as [69]

$$|\mathbf{F}(r)| = \frac{G_N m_1 m_2}{r^2}(1 + \alpha e^{-m_V r}(1 + m_V r)), \qquad (4)$$

where $\alpha \equiv g'^2 q_1 q_2/(4\pi G_N m_1 m_2) = \tilde{q}_1 \tilde{q}_2 > 0$ and r denotes the distance between the two astrophysical objects.

The masses of the NSs are denoted by m_1 and m_2, and the mass of the mediator vector boson is denoted by m_V. The presence of such a new force modifies Kepler's law and the total energy of the system, E_{tot}. The energy loss rate of the system, dE_{tot}/dt, is then determined by the energy loss via gravitational waves, dE_{GW}/dt, and the energy loss via the emission of the new vector particle, dE_V/dt,

$$\frac{dE_{tot}}{dt} = -\frac{d}{dt}(E_{GW} + E_V), \qquad (5)$$

where $dE_V/dt \propto \gamma$ and $\gamma \equiv g'^2(q_1/m_1 - q_2/m_2)^2/(4\pi G_N)$ is the charge-to-mass ratio. Due to the presence of this exotic force, both the plus and the cross polarizations of the GWs are affected. We analytically calculate the GW amplitude and its phase to first order in α and γ. We add post-Newtonian corrections following [77]. To derive the upper limits on α and γ (and therefore g'), we follow the standard Fisher information matrix analysis [78–81]. A complete prescription is given in Appendix B.

IV. BINARY PULSARS

Binary pulsars are a powerful probe of ultralight vectors. In a binary system, the motion of the pulsar and its companion are imprinted in the pulsar time-of-arrival data as an oscillation with a period, P_b, which is typically of $\mathcal{O}(\text{days})$. This is much larger than the pulsar period, which is $\mathcal{O}(\text{msec} - 10 \text{ sec})$. While Keplerian orbits can explain the qualitative motion of a binary pulsar system, the precision of pulsar measurements allows the detection of deviations from classical mechanics due to relativistic effects.

The deviations of a binary pulsar system from simple orbital motion can be described in terms of post-Keplerian parameters [82,83] (see also [66] for a review), the periastron precession, $\dot{\omega}$, the combination of gravitational redshift and Doppler shift, γ_d, as well as the secular drop in the binary period, $\dot{P}_b$, typically of $\mathcal{O}(10^{-12})$. The three parameters depend on different combinations of the pulsar and companion masses. Since measurements of $\dot{\omega}$ and γ_d typically carry a much smaller uncertainty than $\dot{P}_b$, it is natural to use these to fix the masses and use $\dot{P}_b$ to set constraints on new physics as advocated in Ref. [84].

For a binary pulsar system, the large muon abundance leads to the emission of the light $L_\mu - L_\tau$ vector.[4] The subsequent rate of change in the energy of a pulsar relative to gravity is given by [84]

---

[4] In addition, there are relativistic corrections to the force between two NSs which are prominent at slightly higher vector masses than radiation; however, these are subdominant to constraints from ensuring the new force does not eclipse gravity during NS mergers.

$$\frac{\langle \dot{E}_V \rangle}{\langle \dot{E}_{\mathrm{GW}} \rangle} = \frac{5\pi}{12} \gamma \frac{g_V(m_V, \epsilon)}{g_{\mathrm{GR}}(\epsilon)} \left(\frac{P_b}{2\pi G_N (m_1 + m_2)} \right)^{2/3}, \quad (6)$$

where the elliptic correction functions for an eccentricity, ϵ, are

$$g_V(m_V, \epsilon) \equiv \sum_{n > n_0} 2n^2 \left[\mathcal{J}_n'^2(n\epsilon) + \frac{1 - \epsilon^2}{\epsilon^2} \mathcal{J}_n^2(n\epsilon) \right],$$

$$\times \left\{ \sqrt{1 - \frac{n_0^2}{n^2} \left(1 + \frac{1}{2} \frac{n_0^2}{n^2} \right)} \right\} \quad (7)$$

$$g_{\mathrm{GR}}(\epsilon) \equiv \frac{1 + (73/24)\epsilon^2 + (37/96)\epsilon^4}{(1 - \epsilon^2)^{7/2}}, \quad (8)$$

where $\mathcal{J}_n$ is the Bessel function of nth order and $\mathcal{J}_n'$ is its derivative, while the sum begins at $n_0 = m_V P_b / 2\pi$. The observable for each binary pulsar is the ratio of the intrinsic change in the binary orbital period,[5] P_b^{int}, to the prediction from GR, P_b^{GR}. Rewritten in terms of the energy ratios from above yields

$$\frac{\dot{P}_b^{\mathrm{GR}}}{\dot{P}_b^{\mathrm{int}}} = 1 - \frac{\langle \dot{E}_V \rangle}{\langle \dot{E}_{\mathrm{GR}} \rangle}. \quad (9)$$

We are now in a position to set constraints using current pulsar systems. There are many binary pulsars which have by now observed gravitational radiation including pulsar-(nonpulsating) NS binaries [10,15–17,85], a pulsar-pulsar binary [8], pulsar-white dwarf binaries [9,12–14], as well as a pulsar-Oe-type star binary [11]. In setting limits, different systems have different advantages. Since the energy ratio in Eq. (6) is proportional to $P_b^{2/3}$, large orbit binaries are ideal at probing low vector masses. On the other hand, binaries can only emit radiation efficiently if $m_V \lesssim 2\pi/P_b$ leading to smaller binaries becoming effective at probing larger m_V. Furthermore, we note that in order to have significant emission, the binary must carry a dipole moment, requiring the pulsar and its companion to have differing charge-to-mass ratios [as is apparent from the linear dependence of Eq. (6) on the charge-to-mass ratio]. This quantity is maximized in pulsar-white dwarf or pulsar-visible star binaries where the charge of the white dwarf/star is negligible.

To set our constraints on gauged $L_\mu - L_\tau$ using pulsar binaries, we take the 2σ limit on $\dot{P}_b^{\mathrm{int}}/\dot{P}_b^{\mathrm{GR}}$ provided by experiments with the parameters summarized in Fig. 5 of Appendix C.

---

[5]Note that P_b^{int} is the observed value of the period drop which requires subtraction of the effects due to galactic rotation.

V. RESULTS AND DISCUSSION

The constraints on a gauged $U(1)_{L_\mu - L_\tau}$ derived in Secs. III and IV are shown in Fig. 2. The lines marked NS-NS (NS-BH) merger show the sensitivity that could be achieved with a dedicated LIGO/VIRGO analysis using GW170817 (S190814bv). The sensitivity curves in blue and black rely on dipole emission of the vector while the green curve arises from the new force between the two NSs. The right-hand boundaries of both these constraints are functions of f_{ISCO} (frequency of the innermost stable circular orbit). These boundaries lie at different $L_\mu - L_\tau$ vector masses due to the different dependencies of the vector emission (force) on the angular velocity (binary separation) and therefore frequency of the binary. The dipole emission constraint asymptotes to a constant value at small vector masses as the only dependence on the vector mass arises in the step function [see Eq. (B12) in Appendix B]. Finally, the thin (thick) lines of a given color indicate a pessimistic (optimistic) assumption on the muon abundance of the NS involved in the merger (additional details are given in Appendix A).

The constraints shown in red are obtained using current binary pulsar data. We show the envelope of the constraints from all pulsars as the shaded purple region in Fig. 2, while we defer the results for individual pulsars to Fig. 5 of Appendix C. For eccentric binaries, the typical distance between the binaries changes significantly across the orbit and allows vector emission across different masses leading to the observed steplike pattern. Given the pulsar binary separations, the dipole radiation emission is only active for vector masses below $\mathcal{O}(10^{-18} \text{ eV})$. The sensitivity to the gauge coupling is weaker than the equivalent constraints from NS-NS mergers; however, they do not require additional analysis by LIGO and are a present constraint. As such, the binary pulsar constraints serve as a robust alternative to LIGO's GW measurements.

We now consider the validity of the constraints, which were derived assuming the muon number was unaffected by the presence of $L_\mu - L_\tau$. As argued in Sec. II, this approximation breaks down for $g' \gtrsim 10^{-18}$, at which point $N_\mu \propto 1/g'$. However, both the dipole and force effects depend on powers of the combination $g'N_\mu$ which tends to a constant and therefore observable value for $g' > 10^{-18}$. As the dipole emission for NS-NS binaries depends on γ (the difference squared of the respective bodies charge-to-mass ratios), NS-NS binaries that are almost symmetric in charge-to-mass ratios are therefore unobservable irrespective of the gauge coupling size. This also explains the more pronounced difference in sensitivity between the optimistic and pessimistic muon abundances for the NS-NS dipole constraints in Fig. 2 compared to either the force constraints or the NS-BH
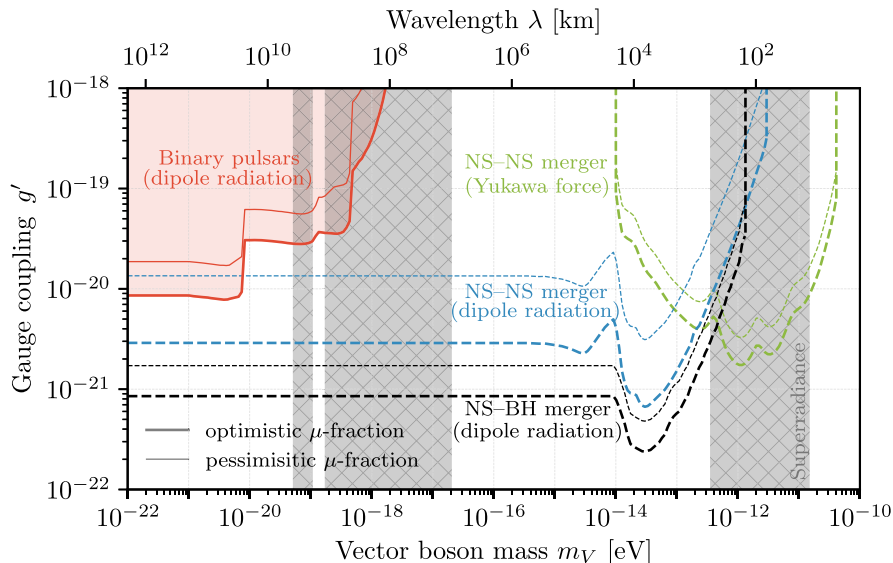
FIG. 2. Current sensitivity of NS binaries to a $L_\mu - L_\tau$ gauge coupling, g', as a function of the vector mass, m_V. The merger curves are projections and require a dedicated analysis to be carried out by the LIGO Collaboration. The gray hatched regions indicate parameter space where the light vector is constrained by BH superradiance considerations [86]. See Sec. V for the discussion of the boundaries of these constraints.

dipole constraints as only one astrophysical body contains muons.

VI. CONCLUSION AND OUTLOOK

We demonstrate the discovery reach to a new muonic force using NSs binary systems. The significant muon abundance inside NSs leads to two new effects: (i) dipole emission of the force mediator and (ii) an additional force between binaries comprising of two NSs. These effects lead to changes in the dynamics of both inspiraling NSs and pulsar binaries. Measuring the deviation in the gravitational waveform and the pulsar period, respectively, are powerful tests of the presence of these new forces. Based on current data and assuming a $U(1)_{L_\mu - L_\tau}$ force as an example, Fig. 2 shows the discovery reach to gauge couplings as small as $\mathcal{O}(10^{-20})$, orders of magnitude better than current probes.

Given the estimated sensitivity of current gravitational wave experiments to these scenarios, we advocate for dedicated studies using improved calculations of the gravitational wave waveform confronted with data from the measured NS-NS merger event GW170817. In addition, future detection of BH-NS events, such as S190814bv, would allow for the isolation of the vector emission.

ACKNOWLEDGMENTS

Note added.—During the preparation of this work, we became aware of [87] which also considered using the muon content in NSs to set constraints on ultralight vectors using pulsar timing data.

APPENDIX A: DEPENDENCE ON NEUTRON STAR EQUATION OF STATE

The exact muon content of a neutron star depends upon the QCD equation of state (EOS) relating the energy density to the pressure in the interior of the neutron star. We base our estimates of the muon content on the most recent Brussels-Montreal EOS [76], which is an update of older works based on the two- and three-nucleon force calculations of [59,76]. These EOS are all compatible with recent limits on the tidal deformability constraints from GW170817 [5,88]. Note, however, that two of these EOS, BSk22 and BSk26, are disfavored due to neutron star cooling measurements. Measurements suggest that relatively few neutron stars exhibit large cooling rates associated with the direct Urca process [89,90]. The former EOS admits direct Urca processes for neutron star masses in excess of $1.151\,M_\odot$, and therefore anomalously large
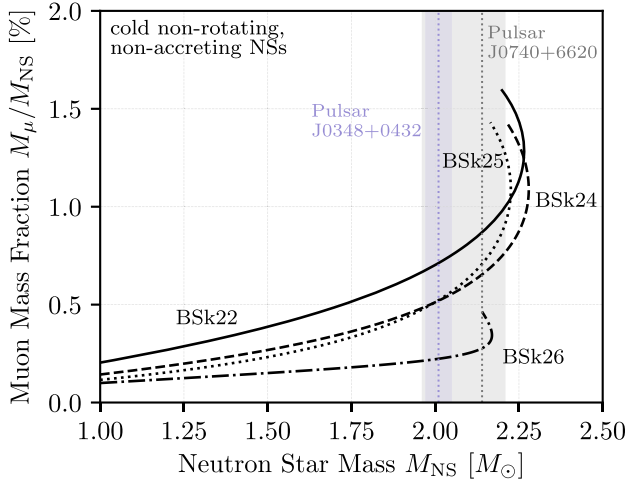
FIG. 3. Muon content of a neutron star as a function of both the mass and EOS. For reference, the two heaviest measured neutron star masses from the NS-WD binary PSR J0348 + 0432 and the millisecond pulsar J0740 + 6620 [94] are shown in purple and gray, respectively.

cooling rates in the majority of the neutron star population [91], while the latter EOS cannot support these processes at all which is in conflict with recent results in [92], suggesting the presence of this process in the neutron star MXB 1659-29. Nevertheless, we take the envelope (shown in Fig. 3) of all four EOSs from [76] as a conservative estimate of the neutron star muon content as a function of the neutron star mass relevant for the different binary systems we consider. Finally, we note that similar EOSs are expected to hold for the description of rapidly rotating neutron star pulsars, while such rotating neutron stars in binary mergers are expected to aid in the extraction of the underlying EOS [93].

To estimate the muon content of the relevant neutron stars, we have utilized the fitting functions from [76] for the relationship between the pressure and density of the neutron star. Based on these fitting functions for the EOS (see Eq. (C4) in [76]), the Tolman-Oppenheimer-Volkof equations can be solved yielding a relation between the mass and density of the neutron star as a function of the radius. To determine the muon abundance, charge neutrality is assumed

$$Y_p = Y_e + Y_\mu, \qquad (A1)$$

as well as equilibrium between the muons and electrons, resulting in chemical potentials that are the same $\mu_e = \mu_\mu$. Here Y_i is the abundance $i = p, e, \mu$ of protons, electrons, and muons defined as $Y_i \equiv n_i/n$ where n is the total density and n_i is the density of the species in question. From the chemical potential, under the assumption of degenerate electron and muon gases as well as sufficiently small $L_\mu - L_\tau$ gauge coupling, we have

$$m_e\left[1 + \frac{(3\pi^2 n_e)^{2/3}}{m_e^2}\right]^{1/2} = m_\mu\left[1 + \frac{(3\pi^2 n_\mu)^{2/3}}{m_\mu^2}\right]^{1/2}, \quad (A2)$$

where m_e and m_μ are the electron and muon masses, respectively. This yields the muon number density

$$n_\mu = \frac{m_e^3}{3\pi^2}\left[1 + \frac{(3\pi^2 n_e)^{2/3}}{m_e^2} - \frac{m_\mu^2}{m_e^2}\right]^{3/2}. \qquad (A3)$$

To evaluate this expression, we take the number density of electrons as a function of neutron density from Eq. (C17) in [76], allowing for the total mass of muons M_μ inside the neutron star to be determined for the different EOSs. The results of which are shown in Fig. 3. We observe that neutron stars with masses greater than a solar mass have $M_\mu \geq 1.5 \times 10^{-3} \, M_{NS}$, while a two solar mass NS would have muon content in the range $0.7 \times 10^{-3} \, M_{NS} \geq M_\mu \geq 0.24 \times 10^{-3} \, M_{NS}$. For reference, we also show the two heaviest observed neutron stars; the NS-WD binary PSR J0348 + 0432 and the millisecond pulsar J0740 + 6620 [94].

APPENDIX B: MODIFICATIONS TO THE GRAVITATIONAL WAVEFORM

Given the force between the two astrophysical objects as denoted by Eq. (2), one can derive the orbital frequency, ω, of the system,

$$\omega^2 = \frac{G_N(m_1 + m_2)}{r^3}[1 - \alpha e^{-m_V r}(1 + m_V r)], \qquad (B1)$$

where the negative sign before α denotes that the force is repulsive. While writing the above equation, we neglect the spins of the astrophysical objects and assume them to be point objects. The orbital frequency is related to the frequency of the gravitational waves, f_{GW}, as $f_{GW} = \omega/\pi$. The total energy of the system can be written as

$$E_{tot} = -\frac{G_N m_1 m_2}{r}(1 - \alpha e^{-m_V r}) + \frac{1}{2}\mu r^2 \omega^2, \quad (B2)$$

where μ denotes the reduced mass of the system. The energy loss rate due to the emission of gravitational waves can be written as

$$\frac{dE_{GW}}{dt} = \frac{32}{5}G_N \mu^2 r^4 \omega^6. \qquad (B3)$$

The energy loss due to the radiation of a light vector particle can be written as

$$\frac{dE_V}{dt} = \frac{2}{3}\gamma\mu^2\omega^4 r^2 \text{Re}\left\{\sqrt{1 - \left(\frac{m_V}{\omega}\right)^2}\left[1 + \frac{1}{2}\left(\frac{m_V}{\omega}\right)^2\right]\right\}, \qquad (B4)$$

where γ is defined below Eq. (3).

Due to the presence of this extra new force and a new way to lose energy from the system, the gravitational wave signature from the merger of two compact astrophysical objects change. The two polarizations of the gravitational waves can be written as [70]

$$h_+(t) = -\left(\frac{1 + \cos^2\iota}{2}\right)\mathcal{A}(t)\cos\left(2\phi_c + 2\phi(t - t_c)\right),$$

$$h_\times(t) = -(\cos\iota)\mathcal{A}(t)\sin\left(2\phi_c + 2\phi(t - t_c)\right). \tag{B5}$$

The inclination angle is denoted by ι, and the time and phase of the system at coalescence is denoted by t_c and ϕ_c. The orbital phase of the system is denoted by ϕ and we will mention how to calculate it later. The amplitude of the signal is denoted by $\mathcal{A}(t)$ where

$$\mathcal{A}(t) = \frac{4G_N}{D_L}\mu\omega^2(t)r^2(t), \tag{B6}$$

where the luminosity distance to the source is denoted by D_L. Given the detector responses, F_+ and $F_\times$, the strain detected by the detector is given by

$$h(t) = F_+ h_+(t + t_c - t_0) + F_\times h_\times(t + t_c - t_0), \tag{B7}$$

$$= -\mathcal{A}(t + t_c - t_0)$$

$$\times \left[\left(\frac{1 + \cos^2\iota}{2}\right)F_+\cos z + (\cos\iota)F_\times\sin z\right], \tag{B8}$$

where $z = 2(\phi_c + \phi(t - t_0))$ and the time in the detector frame when the coalescence is detected is given by t_0. Defining D_{eff} and ϕ_0 such that

$$D_{\text{eff}} = D_L\left[F_+^2\left(\frac{1 + \cos^2\iota}{2}\right)^2 + F_\times^2\cos^2\iota\right]^{-1/2},$$

$$\phi_0 = \phi_c - \arctan\left(\frac{2\cos\iota}{1 + \cos^2\iota}\frac{F_\times}{F_+}\right), \tag{B9}$$

we can write the strain as

$$h(t) = -\frac{4\mu}{D_{\text{eff}}}\omega^2 r^2\cos\left[2\phi_0 + 2\phi(t - t_0; m, \eta)\right]. \tag{B10}$$

In order to determine the upper limits on the parameters α and γ from current observations, we need to determine the Fourier transform of $h(t)$. Using the stationary phase approximation and restricting our calculations to first order in α and γ, we get [70]

$$\tilde{h}(f) = -\sqrt{\frac{5\pi}{24}}G_N^{5/6}\frac{\mathcal{M}^2}{D_{\text{eff}}}(\pi\mathcal{M}f)^{-7/6}\left[\mathcal{A}_{\text{PN}} - \frac{\alpha}{3}C(x) - \frac{5\gamma}{96}(\pi G_N m f)^{-2/3}\Theta\left(\frac{\pi f}{m_V} - 1\right)\right]e^{-i\Psi}, \tag{B11}$$

$$\Psi \equiv 2\pi f t_0 - 2\phi_0 - \frac{\pi}{4} + \frac{3}{128}(\pi G_N\mathcal{M}f)^{-5/3}\left[\frac{20\alpha}{3}F_3(x) - \frac{5\gamma}{84}(\pi G_N m f)^{-2/3}\Theta\left(\frac{\pi f}{m_V} - 1\right)\right] + \Psi_{\text{PN}}, \tag{B12}$$

where $x \equiv G_N^{1/3}mm_V(\pi m f)^{-2/3}$, $m \equiv m_1 + m_2$ is the reduced mass, and the chirp mass is denoted by $\mathcal{M} = \mu^{3/5}(m_1 + m_2)^{2/5}$. The functions $F_3(x)$ and $C(x)$ is defined as

$$F_3(x) = \left(\frac{180 + 180x + 69x^2 + 16x^3 + 2x^4}{x^4}\right)e^{-x} + \frac{21\sqrt{\pi}}{2x^{5/2}}\text{erf}(\sqrt{x}), \tag{B13}$$

$$C(x) = (1 + x - 2x^2)e^{-x}, \tag{B14}$$

where the error function is denoted by $\text{erf}(x)$. Finally, the PN corrections from the gravity-only contribution take the form

$$\Psi_{\text{PN}} = \sum_{n=0}^{4}\frac{3}{128\eta(\pi G_N m f)^{5/3}}\varphi_n(\pi G_N m f)^{n/3}, \tag{B15}$$

$$\mathcal{A}_{\text{PN}} = \sum_{n=0}^{4}\mathcal{A}_n(\pi G_N m f)^{n/3}, \tag{B16}$$

where $\eta \equiv m_1 m_2/m^2$ is the symmetric mass ratio and the coefficients of the sum are given in [77]. We do not include

corrections with $n > 4$ as these additional terms do not significantly alter the presented results.

In order to determine the upper limit on the new physics parameters, α and γ, we follow the Fisher information matrix analysis [78–81]. We denote the dimensionless spin parameters of the two astrophysical objects by χ_1 and χ_2. We define the symmetric and antisymmetric dimensionless spin parameter as $\chi_s = (\chi_1 + \chi_2)/2$ and $\chi_a = (\chi_1 - \chi_2)/2$, respectively. For the Fisher information matrix, we take the underlying parameters to be

$$\boldsymbol{\theta} = \{\log\mathcal{A}, t_c, \phi_c, \log\mathcal{M}_c, \log\eta, \chi_s, \chi_a, \alpha, \gamma\}. \tag{B17}$$
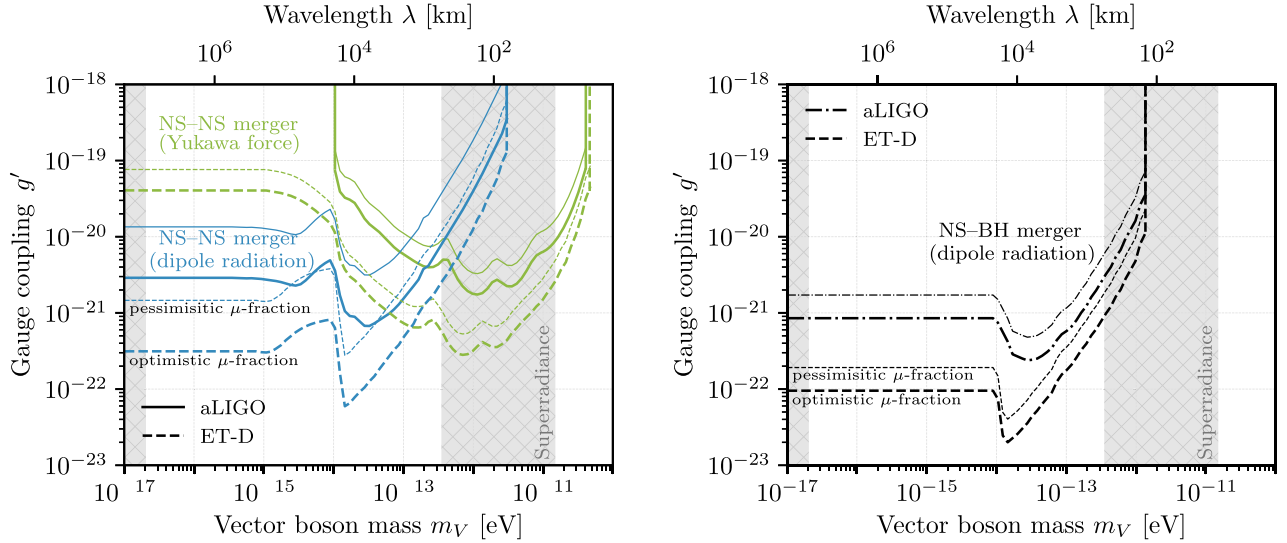
FIG. 4.   Constraints on the gauge coupling g' as a function of the vector mass m_V for a gauged $L_\mu - L_\tau$ symmetry. The regions above the curves indicate the projected parameter space where the presence of the light vector would lead to deviations incompatible with current measurements (solid lines) and future measurements (dashed and dot-dashed lines). Left: projected constraints for an NS-NS event similar to GW170817. Right: projected constraint assuming the observation of an NS-BH merger at a similar luminosity distance to GW170817.

Using these nine parameters, we can construct the 9×9 Fisher information matrix $\mathbf{\Gamma}$ whose components are given by

$$\Gamma_{ab} \equiv \left(\frac{\partial h}{\partial \theta^a} \bigg| \frac{\partial h}{\partial \theta^b} \right), \tag{B18}$$

where a and b run from 1 to 9. The nine parameters, defined in Eq. (B17), are denoted by $\theta^{a,b}$. The inner product is defined as

$$(h_1|h_2) \equiv 4\,\mathrm{Re} \int_{f_\mathrm{low}}^{f_\mathrm{high}} \frac{\tilde{h}_1 \tilde{h}_2^*}{S_n(f')} \mathrm{d}f'. \tag{B19}$$

We choose f_low following [70] and $f_\mathrm{high} = f_\mathrm{ISCO}$, where f_ISCO denotes the frequency of the innermost stable circular orbit [69]. Finally, $S_n(f)$ denotes the spectral noise density of various gravitational wave detectors that we use in our analysis. We use analytical forms of $S_n(f)$ as given in Ref. [70] for the aLIGO and Einstein telescope (ET) sensitivity curves. The signal-to-noise ratio, ρ, is given by

$$\rho \equiv \sqrt{(h|h)}. \tag{B20}$$

We define the covariance matrix, $\mathbf{\Sigma} \equiv \mathbf{\Gamma}^{-1}$. The root-mean-squared error, that can be determined from an observation, for a given parameter θ^a is given by the square root of the (a,a) component of $\mathbf{\Sigma}$. The same expression also gives the 1σ upper limits on the new physics parameters, α and γ,

$$\theta^a_\mathrm{new} \leq \sqrt{\Sigma^{aa}}, \tag{B21}$$

where θ^a_new denotes α and γ.

For the extraction of the 1σ upper limits, we have chosen the parameter values to mimic the observed GW170817 event assuming slowly spinning neutron stars. This corresponds to the choices $m_1 = 1.46\ M_\odot$, $m_2 = 1.27\ M_\odot$ with $\chi_1 = 0.01$ and $\chi_2 = 0.02$. While for the effective luminosity distance, we use $D_\mathrm{eff} = 40$ Mpc. In the left-hand panel of Fig. 4, we show the resulting sensitivity curves for both aLIGO (solid lines) as well as the next generation ground-based experiment ET (dashed lines). In much of the parameter space, ET will improve sensitivity in g' by at least an order of magnitude. We note that the sensitivity curve and therefore resulting sensitivity for Cosmic Explorer is parametrically similar to ET. In the right-hand panel of Fig. 4, we also show the projected sensitivity in the case of the observation of an NS-BH binary merger. Here we assume that $m_1 = M_\mathrm{BH} = 5\ M_\odot$ and $m_2 = M_\mathrm{NS} = 1.46\ M_\odot$, again assuming small spins of both compact objects ($\chi_1 = 0.01$ and $\chi_2 = 0.02$). This type of merger is particularly sensitive as the charge-to-mass ratio is maximized given that BHs carry zero charge under $\mathrm{U}(1)_{L_\mu - L_\tau}$. Subsequently, the constraints are also less sensitive to the uncertainty in the muon content of the neutron star.

APPENDIX C: PULSAR BINARY DATA

The data used to set the binary pulsar constraints is shown in Fig. 5 (left). For a given binary, the necessary

| Pulsar	P_b(day)	$\dot{P}_b^{\rm int}/\dot{P}_b^{\rm GR}$	ϵ	$M_1[M_\odot]$	$M_2[M_\odot]$	Ref
B1913+16(NS)	0.323	0.9983 ± 0.0016	0.617	1.438	1.390	[86]
J0737-3039(P)	0.102	1.003 ± 0.014	0.088	1.3381	1.2489	[8]
J0437-4715(WD)	5.74	1.0 ± 0.1	0.00	1.58	0.236	[9]
B1534+12(NS)	0.421	0.91 ± 0.06	0.274	1.3452	1.333	[10]
B1259-63(O)	1240	1.0 ± 0.5	0.870	1.4	20	[11]
J0348+0432(WD)	0.102	1.05 ± 0.18	0.00	2.01	0.172	[12]
J1141-6545(WD)	0.198	1.04 ± 0.06	0.172	1.27	1.02	[13]
J1738+0333(WD)	0.355	0.94 ± 0.13	0.00	1.46	0.19	[14]
J1756-2251(NS)	0.320	1.08 ± 0.03	0.181	1.341	1.230	[15]
J1906+0746(NS)	0.166	1.01 ± 0.05	0.085	1.291	1.322	[16]
B2127+11C(NS)	0.335	1.00 ± 0.03	0.681	1.358	1.354	[17]
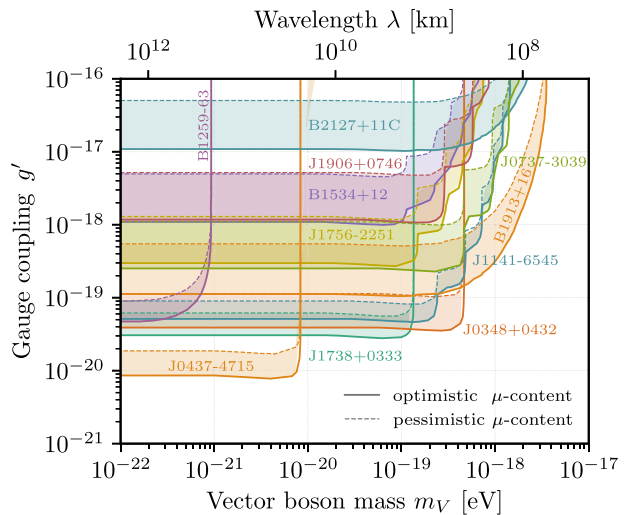
FIG. 5. Data used to set the constraints on gauged $L_\mu - L_\tau$ using pulsar binaries. Left: The parameters for each pulsar relevant for computing the constraints. The type of companion star is shown with the name, denoting a nonpulsating neutron star by NS, pulsar by P, white dwarf by WD, and O as an Oe-type star. Right: Constraints from individual pulsars. For the parameter space above $g' = 10^{-18}$, several new effects as mentioned in Sec. V can become important.

parameters are the binary period, the change in the period relative to that predicted by gravity, the eccentricity, and the masses. We use the neutron star equation of state to compute the muon abundances of the neutron stars as

described in the text. In Fig. 5 (right), we show the constraints from individual pulsar systems with optimistic and pessimistic assumptions on the muon abundance as described in Appendix A.

[1] E. G. Adelberger, B. R. Heckel, and A. E. Nelson, Tests of the gravitational inverse square law, Annu. Rev. Nucl. Part. Sci. **53**, 77 (2003).

[2] J. Murata and S. Tanaka, A review of short-range gravity experiments in the LHC era, Classical Quantum Gravity **32**, 033001 (2015).

[3] E. G. Adelberger, B. R. Heckel, S. A. Hoedl, C. D. Hoyle, D. J. Kapner, and A. Upadhye, Particle Physics Implications of a Recent Test of the Gravitational Inverse Square Law, Phys. Rev. Lett. **98**, 131104 (2007).

[4] S. Schlamminger, K. Y. Choi, T. A. Wagner, J. H. Gundlach, and E. G. Adelberger, Test of the Equivalence Principle Using a Rotating Torsion Balance, Phys. Rev. Lett. **100**, 041101 (2008).

[5] B. P. Abbott et al. (LIGO Scientific and Virgo Collaboration), GW170817: Observation of Gravitational Waves from a Binary Neutron Star Inspiral, Phys. Rev. Lett. **119**, 161101 (2017).

[6] Ligo Scientific and Virgo Collaborations, GCN circular, 25324, https://gracedb.ligo.org/superevents/S190814bv/, 2019.

[7] K. Ackley et al., Observational constraints on the optical and near-infrared emission from the neutron star-black hole binary merger S190814bv, arXiv:2002.01950.

[8] M. Kramer et al., Tests of general relativity from timing the double pulsar, Science **314**, 97 (2006).

[9] W. van Straten, M. Bailes, M. C. Britton, S. R. Kulkarni, S. B. Anderson, R. N. Manchester, and J. Sarkissian, A test of general relativity from the three-dimensional orbital geometry of a binary pulsar, Nature (London) **412**, 158 (2001).

[10] I. H. Stairs, S. E. Thorsett, J. H. Taylor, and A. Wolszczan, Studies of the relativistic binary pulsar psr $b1534 + 12$: I. timing analysis, Astrophys. J. **581**, 501 (2002).

[11] R. M. Shannon, S. Johnston, and R. N. Manchester, The kinematics and orbital dynamics of the PSR B1259-63/LS 2883 system from 23 years of pulsar timing, Mon. Not. R. Astron. Soc. **437**, 3255 (2013).

[12] J. Antoniadis et al., A massive pulsar in a compact relativistic binary, Science **340**, 1233232 (2013).

[13] N. D. R. Bhat, M. Bailes, and J. P. W. Verbiest, Gravitational-radiation losses from the pulsar-white-dwarf binary PSR J1141-6545, Phys. Rev. D **77**, 124017 (2008).

[14] P. C. C. Freire, N. Wex, G. Esposito-Farese, J. P. W. Verbiest, M. Bailes, B. A. Jacoby, M. Kramer, I. H. Stairs, J. Antoniadis, and G. H. Janssen, The relativistic pulsar-white dwarf binary PSR $J1738 + 0333$ II. The most

stringent test of scalar-tensor gravity, Mon. Not. R. Astron. Soc. **423,** 3328 (2012).

[15] R. D. Ferdman *et al.*, PSR J1756-2251: A pulsar with a low-mass neutron star companion, Mon. Not. R. Astron. Soc. **443,** 2183 (2014).

[16] J. van Leeuwen *et al.*, The binary companion of young, relativistic pulsar $J1906 + 0746$, Astrophys. J. **798,** 118 (2015).

[17] B. A. Jacoby, P. B. Cameron, F. A. Jenet, S. B. Anderson, R. N. Murty, and S. R. Kulkarni, Measurement of orbital decay in the double neutron star binary PSR $B2127 + 11C$, Astrophys. J. **644,** L113 (2006).

[18] C. Boehm and P. Fayet, Scalar dark matter candidates, Nucl. Phys. **B683,** 219 (2004).

[19] P. Fayet, Constraints on light dark matter and U bosons, from psi, upsilon, K+, pi0, eta and eta-prime decays, Phys. Rev. D **74,** 054034 (2006).

[20] M. Pospelov, A. Ritz, and M. B. Voloshin, Secluded WIMP dark matter, Phys. Lett. B **662,** 53 (2008).

[21] N. Arkani-Hamed, D. P. Finkbeiner, T. R. Slatyer, and N. Weiner, A theory of dark matter, Phys. Rev. D **79,** 015014 (2009).

[22] M. Goodsell, J. Jaeckel, J. Redondo, and A. Ringwald, Naturally light hidden photons in large volume string compactifications, J. High Energy Phys. 11 (2009) 027.

[23] S. N. Gninenko and N. V. Krasnikov, The muon anomalous magnetic moment and a new light gauge boson, Phys. Lett. B **513,** 119 (2001).

[24] Y. Kahn, M. Schmitt, and T. M. P. Tait, Enhanced rare pion decays from a model of MeV dark matter, Phys. Rev. D **78,** 115002 (2008).

[25] D. Tucker-Smith and I. Yavin, Muonic hydrogen and MeV forces, Phys. Rev. D **83,** 101702 (2011).

[26] B. Batell, D. McKeen, and M. Pospelov, New Parity-Violating Muonic Forces and the Proton Charge Radius, Phys. Rev. Lett. **107,** 011803 (2011).

[27] J. L. Feng, B. Fornal, I. Galon, S. Gardner, J. Smolinsky, T. M. P. Tait, and P. Tanedo, Particle physics models for the 17 MeV anomaly in beryllium nuclear decays, Phys. Rev. D **95,** 035017 (2017).

[28] W. Altmannshofer, S. Gori, M. Pospelov, and I. Yavin, Quark flavor transitions in $L_\mu - L_\tau$ models, Phys. Rev. D **89,** 095033 (2014).

[29] J. A. Dror, R. Lasenby, and M. Pospelov, New Constraints on Light Vectors Coupled to Anomalous Currents, Phys. Rev. Lett. **119,** 141803 (2017).

[30] J. A. Dror, R. Lasenby, and M. Pospelov, Dark forces coupled to nonconserved currents, Phys. Rev. D **96,** 075036 (2017).

[31] R. Laha, B. Dasgupta, and J. F. Beacom, Constraints on new neutrino interactions via light Abelian vector bosons, Phys. Rev. D **89,** 093025 (2014).

[32] P. Arias, D. Cadamuro, M. Goodsell, J. Jaeckel, J. Redondo, and A. Ringwald, WISPy cold dark matter, J. Cosmol. Astropart. Phys. 06 (2012) 013.

[33] M. Escudero, D. Hooper, G. Krnjaic, and M. Pierre, Cosmology with a very light $L_\mu - L_\tau$ gauge boson, J. High Energy Phys. 03 (2019) 071.

[34] W. Altmannshofer, S. Gori, M. Pospelov, and I. Yavin, Neutrino Trident Production: A Powerful Probe of New Physics with Neutrino Beams, Phys. Rev. Lett. **113,** 091801 (2014).

[35] A. Kamada, K. Kaneta, K. Yanagi, and H.-B. Yu, Self-interacting dark matter and muon $g - 2$ in a gauged $U(1)_{L_\mu - L_\tau}$ model, J. High Energy Phys. 06 (2018) 117.

[36] K. Asai, K. Hamaguchi, N. Nagata, S.-Y. Tseng, and K. Tsumura, Minimal gauged $U(1)_{L_a - L_\beta}$ models driven into a corner, Phys. Rev. D **99,** 055029 (2019).

[37] P. Foldenauer, Light dark matter in a gauged $U(1)_{L_\mu - L_\tau}$ model, Phys. Rev. D **99,** 035007 (2019).

[38] G. Arcadi, T. Hugle, and F. S. Queiroz, The dark $L_\mu - L_\tau$ rises via kinetic mixing, Phys. Lett. B **784,** 151 (2018).

[39] M. Bauer, S. Diefenbacher, T. Plehn, M. Russell, and D. A. Camargo, Dark matter in anomaly-free gauge extensions, SciPost Phys. **5,** 036 (2018).

[40] W. Altmannshofer, S. Gori, S. Profumo, and F. S. Queiroz, Explaining dark matter and B decay anomalies with an $L_\mu - L_\tau$ model, J. High Energy Phys. 12 (2016) 106.

[41] A. Biswas, S. Choubey, and S. Khan, Neutrino mass, dark matter and anomalous magnetic moment of muon in a $U(1)_{L_\mu - L_\tau}$ model, J. High Energy Phys. 09 (2016) 147.

[42] J. Heeck and W. Rodejohann, Gauged $L_\mu - L_\tau$ and different muon neutrino and anti-neutrino oscillations: MINOS and beyond, J. Phys. G **38,** 085005 (2011).

[43] J. Heeck and W. Rodejohann, Gauged $L_\mu - L_\tau$ symmetry at the electroweak scale, Phys. Rev. D **84,** 075007 (2011).

[44] J. Alimena *et al.*, Searching for long-lived particles beyond the Standard Model at the Large Hadron Collider, arXiv:1903.04497.

[45] R. Garani and J. Heeck, Dark matter interactions with muons in neutron stars, Phys. Rev. D **100,** 035039 (2019).

[46] A. S. Joshipura, N. Mahajan, and K. M. Patel, Generalised $\mu - \tau$ symmetries and calculable gauge kinetic and mass mixing in $U(1)_{L_\mu - L_\tau}$ models, J. High Energy Phys. 03 (2020) 001.

[47] G. Krnjaic, G. Marques-Tavares, D. Redigolo, and K. Tobioka, Probing Muonic Forces and Dark Matter at Kaon Factories, Phys. Rev. Lett. **124,** 041802 (2020).

[48] I. Galon, E. Kajamovitz, D. Shih, Y. Soreq, and S. Tarem, Searching for muonic forces with the ATLAS detector, Phys. Rev. D **101,** 011701 (2020).

[49] J. A. Grifols and E. Masso, Leptonic photons and nucleosynthesis, Phys. Lett. B **396,** 201 (1997).

[50] A. Kamada and H.-B. Yu, Coherent Propagation of PeV neutrinos and the dip in the neutrino spectrum at IceCube, Phys. Rev. D **92,** 113004 (2015).

[51] S. N. Gninenko, Limit on leptonic photon interactions from SN1987a, Phys. Lett. B **413,** 365 (1997).

[52] N. Bar, K. Blum, and G. D'amico, Is there a supernova bound on axions?, arXiv:1907.05020.

[53] C. D. Kreisch, F.-Y. Cyr-Racine, and O. Doré, The neutrino puzzle: Anomalies, interactions, and cosmological tensions, Phys. Rev. D **101,** 123505 (2020).

[54] A. Yu. Smirnov and X.-J. Xu, The Wolfenstein potential for ultra-light mediators, J. High Energy Phys. 12 (2019) 046.

[55] X. Chu, B. Dasgupta, M. Dentler, J. Kopp, and N. Saviano, Sterile neutrinos with secret interactions—Cosmological discord?, J. Cosmol. Astropart. Phys. 11 (2018) 049.

[56] J. A. Dror, R. Lasenby, and M. Pospelov, Light vectors coupled to bosonic currents, Phys. Rev. D **99,** 055016 (2019).

[57] J. N. Bahcall and R. A. Wolf, Neutron stars. I. Properties at absolute zero temperature, Phys. Rev. **140,** B1445 (1965).

[58] J. N. Bahcall and R. A. Wolf, Neutron stars. II. Neutrino-cooling and observability, Phys. Rev. **140,** B1452 (1965).

[59] A. Y. Potekhin, A. F. Fantina, N. Chamel, J. M. Pearson, and S. Goriely, Analytical representations of unified equations of state for neutron-star matter, Astron. Astrophys. **560,** A48 (2013).

[60] S. Goriely, N. Chamel, and J. M. Pearson, Further explorations of Skyrme-Hartree-Fock-Bogoliubov mass formulas. XII: Stiffness and stability of neutron-star matter, Phys. Rev. C **82,** 035804 (2010).

[61] S. Goriely, N. Chamel, and J. M. Pearson, Further explorations of Skyrme-Hartree-Fock-Bogoliubov mass formulas. XIII. The 2012 atomic mass evaluation and the symmetry coefficient, Phys. Rev. C **88,** 024308 (2013).

[62] J. M. Cohen, W. D. Langer, L. C. Rosen, and A. G. W. Cameron, Neutron star models based on an improved equation of state, Astrophys. Space Sci. **6,** 228 (1970).

[63] N. F. Bell, G. Busoni, and S. Robles, Capture of leptophilic dark matter in neutron stars, J. Cosmol. Astropart. Phys. 06 (2019) 054.

[64] R. Garani, Y. Genolini, and T. Hambye, New analysis of neutron star constraints on asymmetric dark matter, J. Cosmol. Astropart. Phys. 05 (2019) 035.

[65] G. Bertone *et al.*, Gravitational wave probes of dark matter: Challenges and opportunities, arXiv:1907.10610.

[66] R. N. Manchester, Pulsars and gravity, Int. J. Mod. Phys. D **24,** 1530018 (2015).

[67] D. Croon, A. E. Nelson, C. Sun, D. G. E. Walker, and Z.-Z. Xianyu, Hidden-sector spectroscopy with gravitational waves from binary neutron stars, Astrophys. J. **858,** L2 (2018).

[68] L. Sagunski, J. Zhang, M. C. Johnson, L. Lehner, M. Sakellariadou, S. L. Liebling, C. Palenzuela, and D. Neilsen, Neutron star mergers as a probe of modifications of general relativity with finite-range scalar forces, Phys. Rev. D **97,** 064016 (2018).

[69] J. Kopp, R. Laha, T. Opferkuch, and W. Shepherd, Cuckoo's eggs in neutron stars: Can LIGO hear chirps from the dark sector?, J. High Energy Phys. 11 (2018) 096.

[70] S. Alexander, E. McDonough, R. Sims, and N. Yunes, Hidden-sector modifications to gravitational waves from binary inspirals, Classical Quantum Gravity **35,** 235012 (2018).

[71] H. G. Choi and S. Jung, New probe of dark matter-induced fifth force with neutron star inspirals, Phys. Rev. D **99,** 015013 (2019).

[72] M. Fabbrichesi and A. Urbano, Charged neutron stars and observational tests of a dark force weaker than gravity, J. Cosmol. Astropart. Phys. 06 (2020) 007.

[73] A. Hook and J. Huang, Probing axions with neutron star inspirals and other stellar processes, J. High Energy Phys. 06 (2018) 036.

[74] J. Huang, M. C. Johnson, L. Sagunski, M. Sakellariadou, and J. Zhang, Prospects for axion searches with Advanced LIGO through binary mergers, Phys. Rev. D **99,** 063013 (2019).

[75] B. C. Seymour and K. Yagi, Probing massive scalar fields from a pulsar in a stellar triple system, arXiv:1908.03353.

[76] J. M. Pearson, N. Chamel, A. Y. Potekhin, A. F. Fantina, C. Ducoin, A. K. Dutta, and S. Goriely, Unified equations of state for cold non-accreting neutron stars with Brussels–Montreal functionals–I. Role of symmetry energy, Mon. Not. R. Astron. Soc. **481,** 2994 (2018); Erratum, Mon. Not. R. Astron. Soc. **486,** 768 (2019).

[77] S. Khan, S. Husa, M. Hannam, F. Ohme, M. Purrer, X. Jimenez Forteza, and A. Bohe, Frequency-domain gravitational waves from nonprecessing black-hole binaries. II. A phenomenological model for the advanced detector era, Phys. Rev. D **93,** 044007 (2016).

[78] C. M. Will, Testing scalar—tensor gravity with gravitational wave observations of inspiraling compact binaries, Phys. Rev. D **50,** 6058 (1994).

[79] K. Chamberlain and N. Yunes, Theoretical physics implications of gravitational wave observation with future detectors, Phys. Rev. D **96,** 084039 (2017).

[80] M. Vallisneri, Use and abuse of the Fisher information matrix in the assessment of gravitational-wave parameter-estimation prospects, Phys. Rev. D **77,** 042001 (2008).

[81] E. K. Porter and N. J. Cornish, Fisher versus Bayes: A comparison of parameter estimation techniques for massive black hole binaries to high redshifts with eLISA, Phys. Rev. D **91,** 104001 (2015).

[82] T. Damour and N. Deruelle, General relativistic celestial mechanics of binary systems. I. The post-Newtonian motion, Ann. Inst. Henri Poincaré Phys. Théor. **43,** 107 (1985).

[83] T. Damour and N. Deruelle, General relativistic celestial mechanics of binary systems. II. The post-Newtonian timing formula, Ann. Inst. Henri Poincaré Phys. Théor. **44,** 263 (1986).

[84] D. Krause, H. T. Kloor, and E. Fischbach, Multipole radiation from massive fields: Application to binary pulsar systems, Phys. Rev. D **49,** 6892 (1994).

[85] J. M. Weisberg and Y. Huang, Relativistic measurements from timing the binary pulsar PSR $B1913 + 16$, Astrophys. J. **829,** 55 (2016).

[86] M. Baryakhtar, R. Lasenby, and M. Teo, Black hole superradiance signatures of ultralight vectors, Phys. Rev. D **96,** 035019 (2017).

[87] T. K. Poddar, S. Mohanty, and S. Jana, Vector gauge boson radiation from neutron star binaries in a gauged $L_\mu - L_\tau$ scenario, Phys. Rev. D **100,** 123023 (2019).

[88] B. P. Abbott *et al.* (LIGO Scientific and Virgo Collaborations), Properties of the Binary Neutron Star Merger GW170817, Phys. Rev. X **9,** 011001 (2019).

[89] D. Page, J. M. Lattimer, M. Prakash, and A. W. Steiner, Minimal cooling of neutron stars: A new paradigm, Astrophys. J. Suppl. Ser. **155,** 623 (2004).

[90] M. E. Gusakov, A. D. Kaminker, D. G. Yakovlev, and O. Y. Gnedin, Enhanced cooling of neutron stars via cooper-pairing neutrino emission, Astron. Astrophys. **423,** 1063 (2004).

[91] T. Klahn *et al.*, Constraints on the high-density nuclear equation of state from the phenomenology of compact stars and heavy-ion collisions, Phys. Rev. C **74**, 035802 (2006).

[92] E. F. Brown, A. Cumming, F. J. Fattoyev, C. J. Horowitz, D. Page, and S. Reddy, Rapid Neutrino Cooling in the Neutron Star MXB 1659-29, Phys. Rev. Lett. **120**, 182701 (2018).

[93] I. Harry and T. Hinderer, Observing and measuring the neutron-star equation-of-state in spinning binary neutron star systems, Classical Quantum Gravity **35**, 145010 (2018).

[94] H. T. Cromartie *et al.*, Relativistic Shapiro delay measurements of an extremely massive millisecond pulsar, Nat. Astron. **4**, 72 (2019).